Chandra Observations of Coronal Emission from the Early-G Supergiants Alpha and Beta Aquarii

Thomas R. Ayres, Alexander Brown, and Graham M. Harper

Center for Astrophysics and Space Astronomy,
389 UCB, University of Colorado, Boulder, CO 80309-0389;
ayres@casa.colorado.edu, ab@casa.colorado.edu, gmh@casa.colorado.edu

ABSTRACT

We report *Chandra* detections of coronal X-rays from the early-G supergiants α Aquarii (HD209750: G2 Ib) and β Aquarii (HD204867: G0 Ib). Previous *ROSAT* observations of these archetype "hybrid chromosphere" stars were inconclusive in the case of α Aqr, owing to a $38'$ mispointing; and although clearly detecting a source near β Aqr, a small positional discrepancy called the identification into question. The *Chandra* High Resolution Camera (HRC-I), with its superior spatial resolution and sensitivity, has obtained a positive detection of α Aqr, and recovered faint emission at the location of β Aqr, now well separated from the stronger source to the SE that dominated the earlier *ROSAT* image. The coronal $L_{\rm X}/L_{\rm C\ IV}$ luminosity ratios of both supergiants are extremely depressed relative to early-G main sequence stars, continuing the "X-ray deficiency" trend originally identified in late-F/early-G luminosity class III giants of the Hertzsprung gap.

Subject headings: Stars: individual — X-rays: coronae — ultraviolet: spectra

1. INTRODUCTION

Many solar-type dwarf stars are conspicuous "coronal" sources, sporting hot plasma in the range 10^6–10^7 K, and displaying systematic tight correlations of their X-ray luminosity and temperature with rotation rate (Güdel 2004). On the Sun, the multi-million degree gas threads large-scale filamented magnetic "loops" extending high into the tenuous outer atmosphere. The magnetic fields not only trap the hot gas, but are implicated as well in superheating it to more than a hundred times the solar surface temperature. The empirical phenomenology of solar-stellar coronal activity points to a deep-seated magnetic generation mechanism—the dynamo—powered by convection but catalyzed by rotation (Parker 1970).

Decay of the activity over time, evident in comparisons of young clusters of different age, is a signature of angular momentum loss via the coronal wind, which spins down the star thereby suppressing the dynamo action (Skumanich 1972). As a consequence, G-type stars of solar age display considerably diminished coronal X-ray emission compared with their young post–T-Tauri counterparts newly arrived on the MS. The broad coronal behavior of solar-type MS stars thus can be understood in terms of the dynamo, even though its fundamental nature continues to inspire debate among theorists (Stix 2005).

Away from the MS, the story becomes more muddled, even among the stars of solar surface temperature. Late-F/early-G luminosity class III giants in the Hertzsprung gap evolve from 2–3 $M_{\odot}$ late-B/early-A MS stars, and thus have very different convective and rotational histories than solar-mass dwarfs. Gap giants are most active at the end of their lives, rather than at birth; and, although prominent coronal sources, display little if any rotation-activity connection. At the same time, they exhibit a curious "X-ray deficiency" in which $L_{\rm X}/L_{\rm C\,IV}$ luminosity ratios are an order of magnitude depressed from dwarf-star values (Simon & Drake 1989; the C IV $\lambda\lambda$1548,50 doublet, which forms at 10^5 K, is a far-ultraviolet coronal proxy).

Among the G-type supergiants, which have evolved from 5–9 $M_{\odot}$ B-type MS stars, the coronal situation is even more unsettled. On the one hand, there are "active" G supergiants, like β Camelopardalis (HD 31910: G1 Ib-IIa) and β Draconis (HD 159181: G2 Ib-IIa) which are bright sources in the *ROSAT* all-sky survey (RASS) and have solar-like far-UV spectra dominated by high-temperature line emission (e.g., Si IV, C IV, and N V: $T = 0.6$–2×10^5 K). On the other hand, there are "inactive" G supergiants, like α Aquarii (HD 209750: G2 Ib) and β Aquarii (HD 204867: G0 Ib), which were not detected in the RASS, and whose ultraviolet spectra are dominated by low-temperature chromospheric species ($T \sim 1 \times 10^4$ K), like the 1305 Å O I triplet and the 2800 Å Mg II doublet. Contrary to the active supergiants, the chromospheric resonance lines of the inactive objects are cut up by strong blueshifted circumstellar absorptions, apparently from a "wind," slower and cooler than the Sun's coronal outflow, but much larger in mass-loss rate. The inactive G supergiants do display far-UV hot lines like C IV, with broad profiles very similar in shape to those of the active G supergiants, but a factor of five, or so, fainter in surface flux. Hartmann, Dupree, & Raymond (1980) have dubbed the mixed character objects like α Aqr and β Aqr "hybrid chromosphere stars," or "hybrids" for short.

Our *Letter* reports the first definitive X-ray detections of these archetype hybrid G supergiants, made possible by the excellent sensitivity and spatial resolution of *Chandra,* and places the coronal emissions of these objects within the context of other classes of similar-temperature stars, including especially the active G supergiants.

2. Observations

2.1. *Chandra* Targets and Comparison Objects

The main targets of our program were α Aqr and β Aqr. Neither was detected in the RASS, but both were observed during the pointed phase of the *ROSAT* mission. Unfortunately, due to a maneuvering error, α Aqr was placed $38'$ off the boresight, where the imaging is very blurred and detection of faint emission is problematic. The β Aqr observation was fully normal, and a weak point source was found near the predicted position of the hybrid star (Reimers et al. 1996). A subsequent astrometric analysis determined, however, that the β Aqr source was displaced from the predicted target position by $21''$, about a PSPC beam diameter, calling into question the identification as the hybrid star (Ayres 2005).

We also include in the present study the active G supergiants β Cam and β Dra mentioned earlier. These have suitable X-ray material from the RASS and *ROSAT* pointings, and more recently from *XMM*–Newton (β Dra). All four stars have been observed by UV spectrographs on *Hubble* Space Telescope, ensuring accurate measurements of important far-UV emissions such as C IV.

The properties of the four supergiants are summarized in Table 1. The Bright Star Catalog (Hoffleit & Warren 1995) notes that α Aqr and β Aqr are members (with ϵ Pegasi: HD 206778; K2 Ib) of an OB triple system, with space motions nearly perpendicular to the galactic plane. Beta Cam is grouped with the Be star BV Cam (HD 32343: B2.5 Ve) and the eclipsing Algol-type binary DV Cam (HD 34233: B5 V) in the Cas-Tau OB1 association. Alpha Aqr, β Aqr and β Cam have nearly the same bolometric luminosity ($\sim 3 \times 10^3\ L_\odot$) and thus similar masses ($\sim 6.5\, M_\odot$, based on the tracks of Claret [2004]; if the stars are on blue loops, as seems likely since the first-crossing phase is very brief) and ages ($\sim 6 \times 10^7$ y); while β Dra is somewhat less luminous ($\sim 1 \times 10^3\ L_\odot$), less massive ($\sim 5\, M_\odot$) and older ($\sim 1 \times 10^8$ y).

Hydrogen column densities, $N_{\rm H}$, were estimated using an *Extreme Ultraviolet Explorer*–based tool hosted by the Multimission Archive at Space Telescope (MAST), and the appearance of interstellar absorptions in high-resolution ultraviolet spectra. The Aquarii stars have the best determined column, $N_{\rm H} \sim 5 \times 10^{20}$ cm^{-2}, in terms of consistency among the values returned for stars of similar distance or minimum angular separation on the sky. Most of the values returned for stars near β Dra are upper limits, or are unrealistically low with respect to the UV interstellar absorption features of the supergiant. Given the weaker ISM absorptions of β Dra compared with the Aquarii stars, and the fact that β Dra is about half the distance, we adopted $N_{\rm H} \sim 3 \times 10^{20}$ cm^{-2}. The ISM features of β Cam are stronger than those of the Aquarii stars, and α Cam—nearby on the sky but at 3 times the distance

(1 kpc)—indicates $N_{\rm H} \sim 1 \times 10^{21}$ cm^{-2}. We adopted an intermediate value 8×10^{20} cm^{-2} for β Cam.

Color excesses were derived from $N_{\rm H}$ using the conversion $E(B-V) \sim 0.2\,(N_{\rm H})_{21}$ mag (for $N_{\rm H}$ in units of 10^{21} cm^{-2}) from Savage & Mathis (1979: SM79). The resulting values are very similar to those proposed by Schmidt, Rosendhal, & Jewsbury (1974), except for β Dra (0.06 mag here vs. 0.16 mag in the previous study). Extinction corrections were obtained from the color excesses using $A_V \sim 3.1\,E(B-V)$ mag, and $A_{1550\,\text{Å}} \sim 8.14\,E(B-V)$ mag for C IV (SM79). Analogous compensation factors for 0.2–2 keV X-rays were obtained for the several different instruments (e.g., *ROSAT, Chandra, XMM*–Newton) using the WebPIMMS[1] tool available from the High Energy Astrophysics Science Archive Research Center (HEASARC). Bolometric corrections were derived from the $(B-V)_0$ using Table 4 of Flower (1996). The bolometric flux was determined relative to the solar parameters of Bessell, Castelli, & Plez (1998): $f_{\rm bol} \sim 2.54 \times 10^{-5} \times 10^{-(V_0+\text{B.C.})/2.5}$ ergs cm^{-2} s^{-1} at Earth (with B.C.$_\odot \equiv -0.07$ mag).

The influence of $N_{\rm H}$ on the conversion between observed X-ray counts and unabsorbed 0.2–2 keV coronal flux (the so-called Energy Conversion Factor or ECF) is nearly the same as the effect of dereddening $f_{\rm bol}$, so the $L_{\rm X}/L_{\rm bol}$ ratio ($\equiv f_{\rm X}/f_{\rm bol}$) is only minimally altered. (This is true for hot coronal sources, $T \sim 10^7$ K, like β Cam and β Dra based on their PSPC hardness ratios. If the Aquarii coronae are cooler, say $10^{6.5}$ K, then the effect of reddening would become more important.) Conversely, the far-UV extinction is substantially larger than in the optical, thus the $L_{\rm C\ IV}/L_{\rm bol}$ ratio is more strongly affected.

2.2. *Chandra* High Resolution Camera

The *Chandra* X-ray Observatory has been described by Weisskopf, O'Dell, & van Speybroeck (1996); and its HRC-I by Murray et al. (1997). We (Ayres, Brown, & Harper 2003: ABH03) previously used *Chandra* HRC-I to image fields around visually bright, but X-ray faint, red giants. As described in that work, HRC-I has important advantages for detecting weak X-ray emission from optically bright cool stars including: subarcsecond imaging and absolute astrometry ($0\farcs6$ at 90% confidence limits[2]) which minimize source confusion; low cosmic background; and negligible out-of-band response (unlike the CCD cameras of *XMM*–Newton and *Chandra* ACIS which have "red leaks"). The disadvantage of HRC-I

[1]http://legacy.gsfc.nasa.gov/Tools/w3pimms.html

[2]http://asc.harvard.edu/cal/ASPECT

is that, while optimized for high spatial resolution, the microchannel plate camera lacks innate energy discrimination, and thus is unable to spectrally characterize a source. Our objective, however, was to perform a simple exploratory detection experiment: to assess whether sufficient source counts were present to justify a follow-on exposure with one of the energy-resolving CCD imagers, supposing that the red leak problem could be overcome.

2.2.1. HRC-I observations

Alpha Aqr was observed with HRC-I on 2005 January 17 and β Aqr on 2005 April 9, both for 20 ks, as summarized in Table 2. The two HRC-I fields are depicted in Figure 1. Only the extreme inner portions of the $30' \times 30'$ HRC-I images are shown. In the α Aqr field, a single point source appears, coincident with the predicted optical position of the star. In the β Aqr field, on the other hand, two sources are seen: a weaker one at the stellar position, and a stronger one $24''$ to the south east. The latter source, which has more than 80% of the total counts, apparently is the one that dominated the earlier *ROSAT* image (see Ayres 2005, his Figure 2d). Now, the vastly superior spatial resolution of HRC-I has allowed us to unambiguously recover the fainter coronal emission of the hybrid supergiant itself.

2.2.2. HRC-I X-ray Measurements

Based on our previous work with HRC-I (ABH03), and the low backgrounds of the current observations (0.2 counts $[''])^{-2}$), we adopted a detect circle of $r = 0\farcs85$ (85% encircled energy). The expected background in the detect cell thus is <0.5 count; negligible compared with the at least several tens of events recorded in each of the three sources depicted in Fig. 1, rendering even the faintest—β Aqr—a clear detection. The α Aqr and β Aqr sources both fall within $0\farcs2$ of the predicted stellar coordinates, so there is no question concerning the identifications. Measured count rates, and positional offsets, are listed in Table 2.

2.2.3. Additional X-ray (and Far-UV) Measurements

We dearchived X-ray observations of β Cam and β Dra from *ROSAT* for both stars, and *XMM*–Newton for β Dra. We again processed the event lists with custom software, also adopting 85% encircled energy detect cells for the several different cameras (PSPC, HRI, MOS, pn). We obtained *ROSAT* all-sky survey count rates for β Cam and β Dra from the HEASARC "rassbsc" catalog. We also collected far-UV spectra of all four supergiants from

the *HST* archive at MAST. We processed the *HST* spectra using procedures described previously (e.g., ABH03). C IV fluxes were numerically integrated in a 5.5 Å band encompassing both components, above a continuum level based on featureless intervals of the surrounding spectrum. The datasets and results are summarized in Table 3. The final adopted dereddened fluxes are listed in Table 4. For β Cam and β Dra, the X-ray fluxes were divided into independent observations by date (combining all the available measurements on each date, as necessary; e.g., MOS + pn), then averaged.

3. Discussion

Figure 2 places the four supergiants in the context of other early-G stars, in an X-ray/C IV flux-flux diagram. The two shaded areas highlight the locations of G-type MS dwarfs (zone 1: Ayres 1999) and X-ray deficient late-F/early-G Hertzsprung gap giants (zone 2: Ayres et al. 1998). Solar-type dwarfs display a wide range of coronal activity levels, but a tight power-law correlation between X-rays and C IV. Although the data are few, we speculate that the G supergiants fall on a relation parallel to that of the G dwarfs, but as X-ray deficient as—or more so than—the class-III giants. This reinforces the idea that the X-ray deficiency syndrome must be strongly tied to stellar surface gravity, perhaps a systematic influence of the highly extended outer envelopes of evolved stars on fundamental coronal processes (ABH03).

Beyond the striking X-ray deficiency, there still remains the central question of why there is such a large contrast between the active G supergiants and the inactive G-type hybrids. Among G dwarfs, the key governing parameter would be rotation, but like the class-III early-G gap giants, rotation does not appear to be an important activity discriminant among the four supergiants of our study (which have essentially identical $v \sin i$: Table 1). It is possible that the surface layers are decoupled from the deep interior where the magnetic flux is generated (e.g., Gray & Toner 1987), so the photospheric $v \sin i$ is not a clean measure of the true internal angular momentum state that feeds the stellar dynamo. Perhaps, also, the internal angular momentum of certain supergiants is enriched at the red giant tip by engulfment of a close stellar companion (Siess & Livio 1999). Unfortunately, neither of these possibilities would be straightforward to test. Thus, the activity instigator for the G supergiants remains an open question.

4. For the Future

Now that α Aqr and β Aqr have been positively detected by HRC-I, the next step is to measure their coronal temperatures using one of the CCD-based instruments, such as *Chandra* ACIS-I (which is less susceptible to red leak than backside-illuminated ACIS-S). Among G-type dwarfs, coronal temperatures increase systematically with increasing $L_{\rm X}/L_{\rm bol}$ (Telleschi et al. 2005), and we already know that the spectra of the two active G supergiants are very hot. The possibility exists that like dwarfs, the coronal temperatures of the G supergiants cool off with decreasing activity; which could have a significant impact on inferring the unabsorbed coronal fluxes, and evaluating the degree of X-ray deficiency.

Another obvious direction would be to boost the G supergiant sample in numbers to establish whether the X-ray/C IV trend in Fig. 2 is real, or an accident of limited statistics. The large X-ray deficiency of the G supergiants makes this a formidable task, not helped by the relative rarity of that stellar class. Nevertheless, these objects clearly have an important statement to make concerning the extremes of coronal activity in the H–R diagram, and decoding that message might uncover important clues to understanding the more familiar, but still enigmatic, solar dynamo.

This work was supported by *Chandra* grant G05-6010X from the Smithsonian Astrophysical Observatory, and NASA grant NAG5-13058. Observations from the *Chandra* X-ray Observatory were collected and processed at the *Chandra* X-ray Observatory Center, operated for NASA by Smithsonian Astrophysical Observatory. This research also utilized the SIMBAD database, maintained by *CDS*, Strasbourg, France; the *ROSAT* and *XMM*–Newton public archives at the HEASARC of the NASA Goddard Space Flight Center; and *HST* data from the Multimission Archive at Space Telescope (MAST), including the "Cool-CAT" cool-star spectral catalog. We also made use of the X-ray count-rate tool provided by HEASARC and the hydrogen column density calculator hosted by MAST.

Table 1. Target Stars and Comparison Objects

Star Name	HD No.	Type	V	$B-V$	d	$N_{\rm H}$	$E(B-V)$	$v \sin i$
			(mag)		(pc)	(10^{20} cm^{-2})	(mag)	(km s^{-1})
α Aqr	209750	G2 Ib	2.95	0.96	230±50	5	0.10	6.7 ± 1.5
β Aqr	204867	G0 Ib	2.91	0.83	190±40	5	0.10	6.3 ± 1.3
β Cam	31910	G1 Ib-IIa	4.03	0.87	310±70	8	0.16	8.5 ± 1.3
β Dra	159181	G2 Ib-IIa	2.79	0.98	110±6	3	0.06	7.3 ± 0.5

Note. — Stellar parameters from SIMBAD; except types from Keenan & McNeil (1989), and rotational velocities from Gray & Toner (1987).

Table 2. *Chandra* HRC-I Observations

Name	ObsID	UT Start (yyyy-mm-dd)	$t_{\rm exp}$ (ks)	$C_{\rm X}$ (counts ks^{-1})	$(\Delta x, \Delta y)$ (arcseconds)
α Aqr	5414	2005-01-17	18.20	6.3 ± 0.6	(0.0,+0.1)
β Aqr	5413	2005-04-09	20.15	1.7 ± 0.3	(+0.1,0.0)
β Aqr SE source	···	···	···	8.9 ± 0.7	(+12.4,−21.1)

Note. — $t_{\rm exp}$ refers to total of the "good time" intervals: 2 ks of the α Aqr observation were corrupted by high background radiation and excluded. Errors are $1\,\sigma$. Positional offsets are relative to predicted stellar coordinates at the epoch of observation: measurement errors are smaller than the $\pm 0\farcs6$ associated with the aspect reconstruction.

Table 3. Additional UV and X-ray Measurements

Name	Instrument	Dataset	UT Start (yyyy-mm-dd)	$t_{\rm exp}$ (ks)	$f_{\rm C\,IV}$, $f_{\rm X}$(0.2–2 keV) (10^{-12} ergs cm^{-2} s^{-1})	Notes
α Aqr	HST/GHRS	z1fg010am	1993-07-10	4.79	0.498 ± 0.008	C= 0.02
β Aqr	HST/STIS	o5bn5001,2;5104,5	2000-04-16;28	17.48	0.285 ± 0.004	C= 0.01
β Cam	HST/STIS	o5bn6001	1999-09-19	13.75	0.505 ± 0.005	C= 0.01
···	ROS/PSPC	rassbsc	1990-08-15	0.43	0.9 ± 0.1	ECF= 13
···	ROS/PSPC	rp201221n00	1992-09-25	4.71	0.86 ± 0.05	ECF= 13
···	ROS/HRI	rh202530n00	1997-08-31	2.51	0.8 ± 0.1	ECF= 32
β Dra	HST/GHRS	z0wz010ft	1992-04-23	0.90	2.52 ± 0.04	C= 0.05
···	···	z1gb0107t	1993-02-20	0.90	2.51 ± 0.04	C= 0.05
···	···	z2nw010ct	1995-04-30	0.90	2.40 ± 0.04	C= 0.05
···	ROS/PSPC	rassbsc	1990-07-30	1.32	3.5 ± 0.2	ECF= 11
···	ROS/PSPC	rp180282n00	1998-12-15	1.16	3.1 ± 0.2	ECF= 11
···	XMM/MOS	0021750201	2002-09-28	7.36	4.5 ± 0.1	ECF= 9
···	XMM/pn	···	···	6.05	5.0 ± 0.1	ECF= 3
···	XMM/MOS	0021751001	2002-09-30	6.80	4.4 ± 0.1	ECF= 9
···	XMM/pn	···	···	7.05	4.9 ± 0.1	ECF= 3
···	XMM/pn	0021751101	2002-10-06	2.73	4.7 ± 0.1	ECF= 3

Note. — In Notes column, "C" refers to a background continuum subtracted from the C IV doublet, in 10^{-12} ergs cm^{-2} s^{-1} Å^{-1}, and "ECF" refers to the X-ray energy conversion factor in 10^{-12} ergs cm^{-2} count^{-1} (into 0.2–2 keV band). Errors are $1\,\sigma$.

Table 4. De-Reddened Fluxes

Star Name	$f_{\rm bol}$ (10^{-7} ergs cm^{-2} s^{-1})	$f_{\rm C\,IV}$ (10^{-14} ergs cm^{-2} s^{-1})	$f_{\rm X}$
α Aqr	26.8	105 ± 2	5.7 ± 0.5
β Aqr	25.9	60 ± 1	1.5 ± 0.3
β Cam	10.9	167 ± 2	85 ± 5
β Dra	25.9	389 ± 11	420 ± 80

REFERENCES

Ayres, T. R. 1999, ApJ, 525, 240

_____. 2005, ApJ, 618, 493

Ayres, T. R., Brown, A., & Harper, G. M. 2003, ApJ, 598, 610 (ABH03)

Ayres, T. R., Simon, T., Stern, R. A., Drake, S. A., Wood, B. E., & Brown, A. 1998, ApJ, 496, 428

Bessell, M. S., Castelli, F., & Plez, B. 1998, A&A, 333, 231

Claret, A. 2004, A&A, 424, 919

Flower, P. J. 1996, ApJ, 469, 355

Güdel, M. 2004, A&A Rev., 12, 71

Hartmann, L., Dupree, A. K., & Raymond, J. C. 1980, ApJ, 236, L143

Hoffleit, D., & Warren, W. H. 1995, VizieR Online Data Catalog, 5050, 0

Keenan, P. C., & McNeil, R. C. 1989, ApJS, 71, 245

Murray, S. S., et al. 1997, Proc. SPIE, 3114, 11

Parker, E. N. 1970, ARA&A, 8, 1

Reimers, D., Huensch, M., Schmitt, J. H. M. M., & Toussaint, F. 1996, A&A, 310, 813

Savage, B. D., & Mathis, J. S. 1979, ARA&A, 17, 73 (SM79)

Schmidt, E. G., Rosendhal, J. D., & Jewsbury, C. P. 1974, ApJ, 189, 293

Siess, L., & Livio, M. 1999, MNRAS, 304, 925

Simon, T., & Drake, S. A. 1989, ApJ, 346, 303

Skumanich, A. 1972, ApJ, 171, 565

Stix, M. 2005, Astronomische Nachrichten, 326, 155

Telleschi, A., Güdel, M., Briggs, K., Audard, M., Ness, J., & Skinner, S. L. 2005, ApJ, 622, 653

Weisskopf, M. C., O'Dell, S. L., & van Speybroeck, L. P. 1996, Proc. SPIE, 2805, 2

Fig. 1.— (a) HRC-I observation of α Aqr. The circle indicates the 85% encircled energy detect cell ($r = 0\farcs85$). The ordinate and abscissa are relative to the predicted position of the star (marked by the cross). (b) Same for β Aqr. Here, a weak source appears at the stellar position, but a second, stronger source lies $24''$ to the south east. The latter dominated the earlier lower resolution *ROSAT* PSPC field.

Fig. 2.— X-ray/C IV flux-flux diagram. Normalization by the bolometric fluxes removes the twin biases of different distances and diameters. Shaded zones represent: (1) early-G dwarfs ("$\odot$" marks cycle-average solar ratio); and (2) "X-ray deficient" late-F/early-G class-III giants in the Hertzsprung gap. The box at upper left indicates corrections for reddening of 0.1 mag for two values of the coronal temperature.

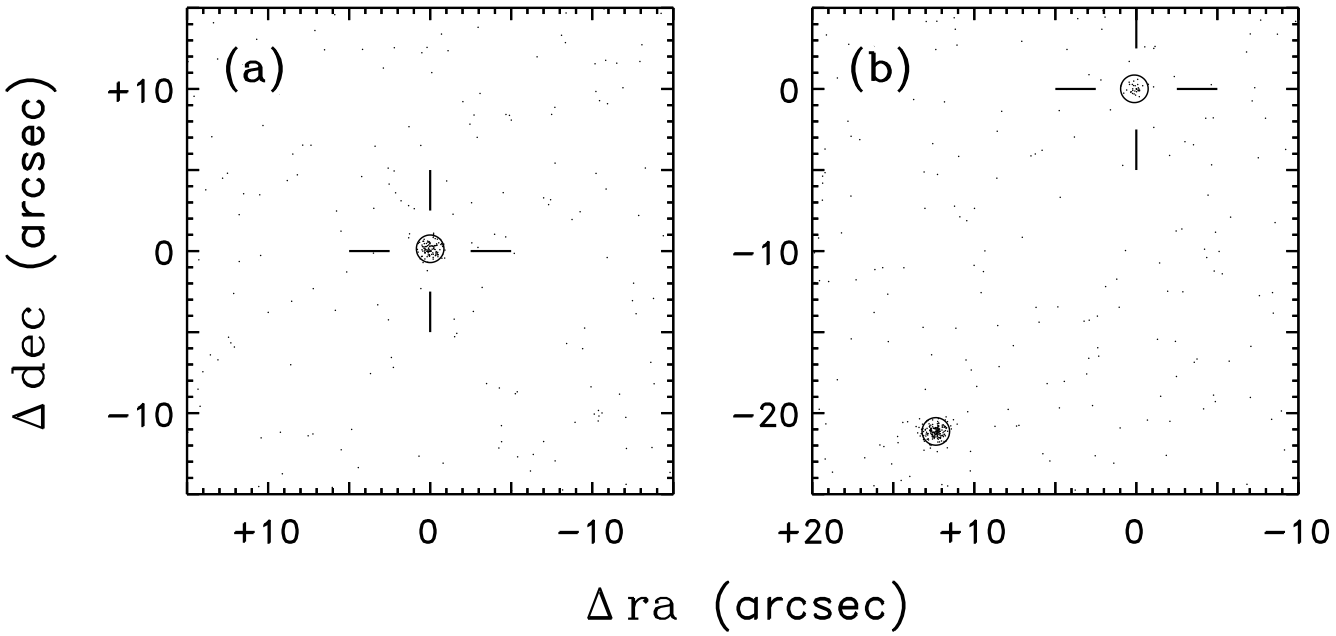

Fig. 1.—

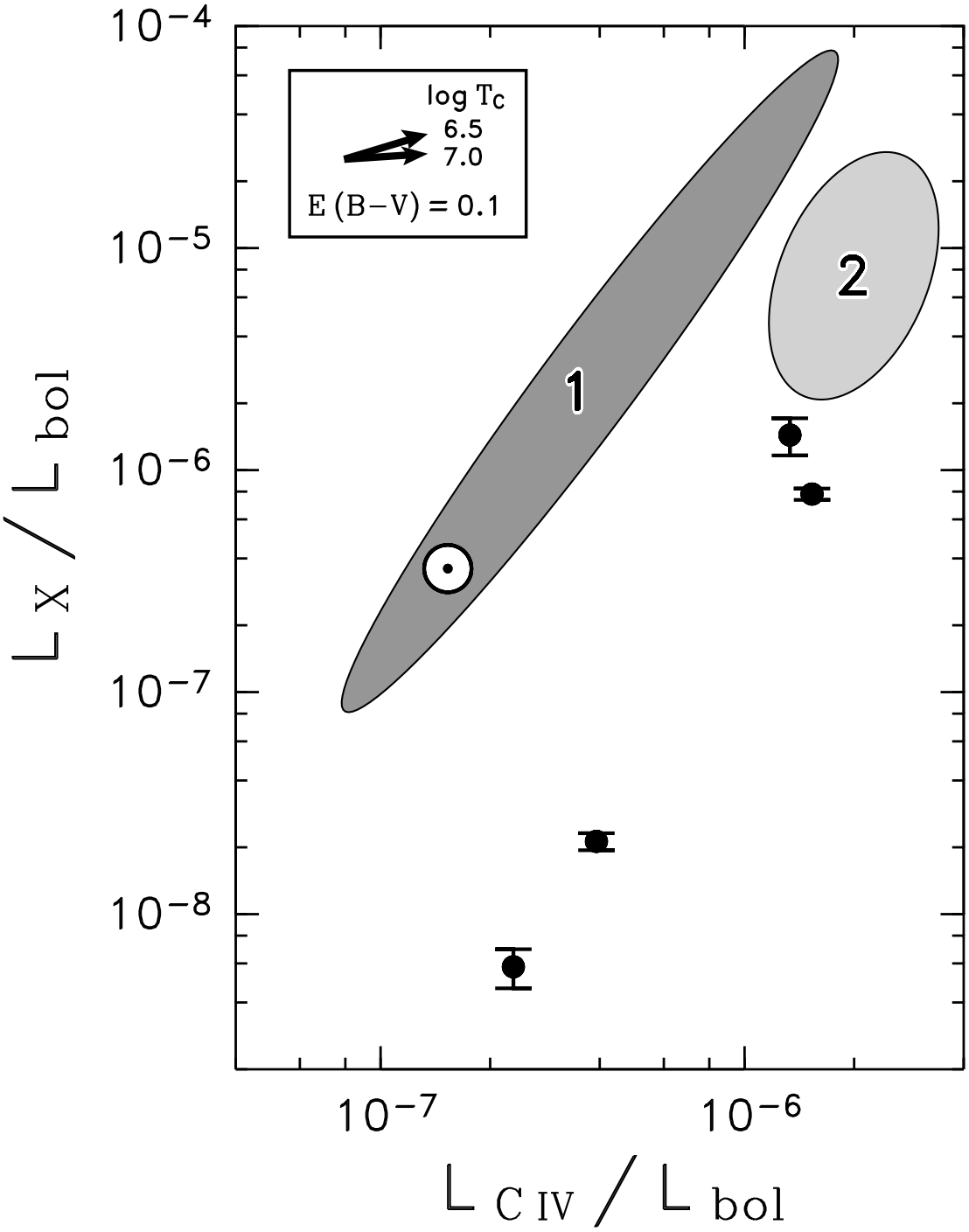
log Tc
6.5
7.0
E (B−V) = 0.1
1
2
10−4
10−5
10−6
10−7
10−8
10−7
10−6
L X / L bol
L C IV / L bol

Fig. 2.—